Soheil Hatami, Christian Würth, Martin Kaiser, Susanne Leubner, Stefanie Gabriel, Lydia Bahrig, Vladimir Lesnyak, Jutta Pauli, Nikolai Gaponik, Alexander Eychmüller, Ute Resch-Genger

Absolute photoluminescence quantum yields of IR26 and IR-emissive Cd1–xHgxTe and PbS quantum dots – method- and material-inherent challenges

Erstveröffentlichung in / First published in:
Nanoscale. 2015, 7(1), S. 133–143 [Zugriff am: 04.11.2019]. Royal Society of Chemistry. ISSN 2040-3372.

DOI: https://doi.org/10.1039/c4nr04608k

Nanoscale

PAPER

View Article Online
View Journal | View Issue

Cite this: *Nanoscale*, 2015, **7**, 133

Absolute photoluminescence quantum yields of IR26 and IR-emissive $Cd_{1-x}Hg_xTe$ and PbS quantum dots – method- and material-inherent challenges†

Soheil Hatami,[a] Christian Würth,[a] Martin Kaiser,[a] Susanne Leubner,[b] Stefanie Gabriel,[b] Lydia Bahrig,[b] Vladimir Lesnyak,[b,c] Jutta Pauli,[a] Nikolai Gaponik,[b] Alexander Eychmüller[b] and Ute Resch-Genger*[a]

Bright emitters with photoluminescence in the spectral region of 800–1600 nm are increasingly important as optical reporters for molecular imaging, sensing, and telecommunication and as active components in electrooptical and photovoltaic devices. Their rational design is directly linked to suitable methods for the characterization of their signal-relevant properties, especially their photoluminescence quantum yield (Φ_f). Aiming at the development of bright semiconductor nanocrystals with emission >1000 nm, we designed a new NIR/IR integrating sphere setup for the wavelength region of 600–1600 nm. We assessed the performance of this setup by acquiring the corrected emission spectra and Φ_f of the organic dyes Itrybe, IR140, and IR26 and several infrared (IR)-emissive $Cd_{1-x}Hg_xTe$ and PbS semiconductor nanocrystals and comparing them to data obtained with two independently calibrated fluorescence instruments absolutely or relative to previously evaluated reference dyes. Our results highlight special challenges of photoluminescence studies in the IR ranging from solvent absorption to the lack of spectral and intensity standards together with quantum dot-specific challenges like photobrightening and photodarkening and the size-dependent air stability and photostability of differently sized oleate-capped PbS colloids. These effects can be representative of lead chalcogenides. Moreover, we redetermined the Φ_f of IR26, the most frequently used IR reference dye, to 1.1×10^{-3} in 1,2-dichloroethane DCE with a thorough sample reabsorption and solvent absorption correction. Our results indicate the need for a critical reevaluation of Φ_f values of IR-emissive nanomaterials and offer guidelines for improved Φ_f measurements.

Received 11th August 2014,
Accepted 24th October 2014

DOI: 10.1039/c4nr04608k

www.rsc.org/nanoscale

1 Introduction

Fundamental advances in biochemical assays, molecular sensors, optical imaging, telecommunication, and optical, electroluminescent, and photovoltaic devices require bright and stable fluorophores.[1–7] A straightforward measure of fluorophore performance is the photoluminescence quantum yield (Φ_f),[8,9] given by the number of emitted photons N_{em} per number of photons N_{abs} absorbed by the system, see eqn (1).[9–11] For fluorescent nanomaterials such as semiconductor nanocrystals (NCs), *i.e.*, quantum dots and rods,[8] and for upconversion nanocrystals (NCs),[12,13] where surface states and the accessibility of emissive states by quenchers largely control the accomplishable Φ_f values,[14–18] the value of Φ_f provides also a straightforward tool to assess the quality of the surface shell and surface passivation and hence to evaluate new synthetic and surface functionalization strategies.[19] Moreover, concentration-dependent Φ_f gives a direct hint of ligand desorption as recently shown for, *e.g.*, CdTe and CdSe quantum dots,[14,15,20–22] which is typically the first step to material decomposition, resulting in the release of toxic heavy metal ions.[8,20,23]

$$\Phi_f = \frac{N_{em}(\lambda)}{N_{abs}(\lambda)} \quad (1)$$

Φ_f can be obtained directly by optical methods either relative to a fluorescent reference with known Φ_f or as an absolute quantity (standard-free),[9,11,24,25] or by calorimetric methods like photoacoustic spectroscopy and thermal lensing.[26–28]

[a]*BAM Federal Institute for Materials Research and Testing, Richard-Willstaetter-Str. 11, 12489 Berlin, Germany. E-mail: ute.resch@bam.de*
[b]*Physical Chemistry and Center for Advancing Electronics Dresden, TU Dresden, Bergstr. 66b, 01062 Dresden, Germany*
[c]*Department of Nanochemistry, Istituto Italiano di Tecnologia, via Morego, 30, 16163 Genova, Italy*

†Electronic supplementary information (ESI) available. See DOI: 10.1039/c4nr04608k

Commonly, Φ_f is obtained optically, comparing the absorption-weighted integral fluorescence intensities of a sample and a reference measured under identical conditions.[9,11,24] Due to the need for standards with reliably known Φ_f, this straightforward procedure is limited predominantly to the ultraviolet (UV), visible (vis) and NIR regions, where Φ_f standards have been recommended for many years[9,24,25,27–32] or were recently provided by us.[9,25] This included the reevaluation of Φ_f of IR125 in dimethylsulfoxide (DMSO), the most frequently used NIR reference dye for organic fluorophores and semiconductor NCs,[33–37] yielding a Φ_f of 0.23[9] instead of the previously assumed Φ_f of 0.13,[38] and consequently, an underestimation of all Φ_f values obtained relative to this dye. Nevertheless, the accurate determination of Φ_f > 1000 nm still presents a considerable challenge as indicated by the recently reexamined Φ_f of the most frequently used IR Φ_f reference dye IR26,[39–42] demonstrating large deviations in its Φ_f in 1,2-dichloroethane (DCE) by a factor of up to 10.[43–45] This was recently addressed in depth by the absolute measurements of its Φ_f by Semonin *et al*. using a self-made integrating sphere setup.[43] These high uncertainties in the red wavelength region originate from the fact that many critical issues affecting especially photoluminescence measurements in the IR wavelength region, such as the performance and validation of instrument calibrations,[46] solvent and water vapor absorption, and sample reabsorption,[24,47,48] have not been really detailed so far. Moreover, semiconductor NC-specific effects like material- and surface chemistry-dependent photodecomposition and photobrightening,[8,14,49] which can depend on the incident spectral radiant flux and even on the NC size, or a possible excitation wavelength dependence of Φ_f[50,51] were not addressed.

Aiming at the rational design of bright NIR- and IR-emissive semiconductor NCs with emission in the wavelength region of 650–1600 nm and to address the relevance of the reliable characterization of emerging luminescent reporters for the NIR II window of 1000–1700 nm for, *e.g.*, bioimaging studies,[52–54] we present the design of a new integrating sphere setup for absolute measurements of photoluminescence spectra and Φ_f from 600 to 1600 nm and its calibration and performance validation. Subsequently, we reexamined the Φ_f of IR26 and quantified measurement uncertainties. Then, we measured Φ_f of representative NIR- and IR-emissive semiconductor NCs, here $Cd_{1-x}Hg_xTe$ colloids with size and composition tuning of the optical and electrochemical properties,[42,55,56] and differently sized PbS, presenting the most commonly used NCs in photovoltaics,[3,33,57] to provide examples of achievable Φ_f values.

2 Methods

2.1 Reagents and materials

The Φ_f standards HITCI (batch number 029006) and IR125 (batch number 10970) used for relative measurements and IR140 (batch number 9310) were obtained from Lambda Physics, the spectral emission standard Itrybe from Otava (batch number OTVD_0037), and IR26 from Acros (batch number 409401000). The chemical structures are given in the ESI† (Fig. 1S). The solvents used for the spectroscopic studies, *i.e.*, ethanol for Itrybe and HITCI, dimethylsulfoxide (DMSO) for IR125 and IR140, 1,2-dichloroethane (DCE) for IR26, and tetrachloroethylene (TCE) for PbS, were of spectroscopic grade and were purchased from Sigma Aldrich and Merck. For $Cd_{1-x}Hg_xTe$, deuterated water (D_2O) from Merck was employed.

2.2 Synthesis of semiconductor NCs

$Cd_{1-x}Hg_xTe$ of different compositions and sizes were synthesized in water as previously described using mercaptopropionic acid (MPA) as a ligand[42] and stored in the dark in air. Differently sized PbS colloids were prepared according to Poppe *et al.*[58] under inert gas, purified, and stored as stock solutions in toluene either in a glove box or under an inert gas atmosphere or in air in the dark in the refrigerator.

2.3 Characterization

Dye purity was determined by high performance liquid chromatography (HPLC) with the Agilent 1200 HPLC system (Agilent) using a previously reported method[25] and yielded the following purities (100% method): HITCI: 97.9% (760 nm),[25] IR125: 99.1% (800 nm),[25] Itrybe: 99.8% (600 nm), IR140: 90.2% (700 nm), and IR26: 99.5% (750 nm). The size of the PbS NCs was determined from absorption spectra to be 2.3 nm, 4.1 nm, and 4.4 nm, respectively, as described by Cademartiri *et al.*[59] The size and composition of the $Cd_{1-x}Hg_xTe$ NCs was determined to be 4.8 nm, 6.3 nm, and 7.1 nm for colloids with Cd : Hg ratios of 99 : 1, 98 : 2, and 97 : 3, respectively, using TEM and ICP-OES. Absorption spectra were recorded on a calibrated Cary 5000 spectrometer. Fluorescence emission spectra and Φ_f were measured with a FSP920 spectrofluorometer (Edinburgh Instruments; 300–1700 nm; relative measurements with HITCI (Φ_f = 0.30; ethanol) and IR125 (Φ_f = 0.23; DMSO) as the references),[9,24,25] a custom made UV/vis/NIR integrating sphere setup (350–1050 nm),[25] and our newly designed NIR/IR integrating sphere setup (600–1600 nm), all independently calibrated (see ESI† for details of instrumentation and calibration including the transfer standards employed). All absorption and fluorescence measurements were performed with freshly prepared dye or NC solutions (absorbances A of 0.02 to 0.1 at the longest wavelength absorption maximum or the first excitonic peak) at T = (25 ± 1) °C in air using either 10 mm × 10 mm quartz cuvettes from Hellma GmbH or 10 mm × 4 mm cells to minimize dye or NC reabsorption and/or solvent absorption. For IR26, absorbances of up to 0.8 were used. Stock solutions of $Cd_{1-x}Hg_xTe$ NC stored in air in the dark at room temperature were diluted with D_2O by a factor of at least 1000 : 1 before each measurement. For potentially air-sensitive PbS colloids, aging studies were performed with the stock solutions of the three PbS colloids in toluene, stored in air in the dark in the refrigerator. To representatively address the influence of oxygen, the 4.4 nm sized PbS NC batch was split into two portions, one kept always under inert gas in the dark at room temperature and the other one under

identical conditions to the stock solutions of the smaller PbS colloids. For the spectroscopic studies, the PbS stock solutions were always diluted by a factor of at least 1000 : 1 with TCE and measured in air, except for 4.4 nm PbS stored and aged under inert gas. In this case, TCE dilution was performed in a glove box and sealed cells were used for subsequent spectroscopic measurements. All fluorescence emission spectra shown were blank-corrected and corrected for instrument-specific effects relative to the spectral photon radiance scale.[46,60,61] Relative standard deviations of fluorescence measurements were obtained from four independent measurements. Spectral corrections such as a reabsorption correction[9,24,25] and solvent absorption correction are detailed in the ESI.†

3 Results and discussion

3.1 Design of an integrating sphere setup for the NIR and IR

The design of our integrating sphere setup for absolute Φ_f measurements from 600 to 1600 nm with versatile excitation, reasonable spectral resolution, and high sensitivity is shown in Fig. 1 (for more details of setup components, see ESI†). To optimize the sensitivity of the setup, which should enable the determination of not only the moderate to high Φ_f of semiconductor NCs exceeding 0.1, but also those of organic dyes with emission >1000 nm like IR26 with very small $\Phi_f < 5 \times 10^{-3}$,[43] we chose a small integrating sphere (diameter of *ca.* 11 cm) with a high reflectivity hydrophobic Spectralon coating (99% from 400 to 1500 nm) as the sample compartment, thereby minimizing water adsorption from air. This sphere, which is large enough to minimize distortions of the radiating field in the sphere by the sample, was equipped with six ports for sample illumination, positioning of the sample holder, emission detection, and purging with dry nitrogen to remove water vapor absorbing at around 950 nm, 1130 nm, and 1450 nm (see ESI, Fig. 7S†). This avoids distortions of the measured transmitted excitation light and photoluminescence, which become otherwise dependent on air humidity (and ambient temperature) and optical path length. As excitation light sources, we chose different high stability (intensity fluctuations <1%; see ESI†) intense lasers (HeNe laser: 633 nm), laser diodes (690 nm, 730 nm, 785 nm, 808 nm, and 980 nm), and a diode-pumped solid-state laser (914 nm), to enable the measurement of dye and NC samples absorbing and emitting over a broad wavelength region with strongly varying photoluminescence efficiencies. These light sources were coupled *via* fiber optics (Fig. 1, top) to the integrating sphere (Fig. 1, bottom) or directed either directly into the middle of the sphere (sample position) or on the sphere wall with a flat mirror. This enables direct and indirect sample illumination and their combination.[62] The small spot diameters of 1–4 mm of these excitation light sources provide control of the illuminated volume to minimize solvent absorption and reabsorption effects. This is of special relevance for the measurement of solutions and dispersions >950 nm due to the absorbance of many solvents and matrices in this wavelength region

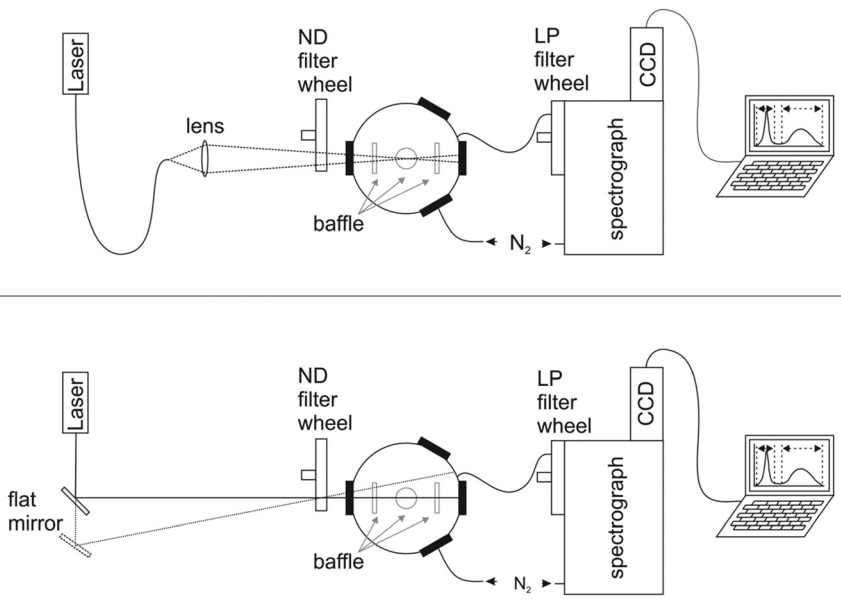

Fig. 1 NIR/IR integrating sphere setup for absolute measurement of photoluminescence in the wavelength region of 600 nm to 1600 nm consisting of several high stability (intensity fluctuations <1%) lasers and laser diodes, coupled either *via* fiber optics (upper panel; 808 and 980 nm laser diodes) or directly (HeNe laser, 690 nm, 730 nm, and 785 nm laser diodes; 914 nm solid-state laser) with a flat mirror (lower panel) to a N_2-purged 12 cm integrating sphere attached *via* an IR-quartz fiber bundle to an imaging spectrograph equipped with an InGaAs CCD. The mirrors can be used for direct or indirect sample illumination. Two filter wheels, one equipped with neutral density (ND) filters placed between the sphere and the light sources, and one equipped with different long pass (LP) interference filters (cut-on wavelengths of 600, 800, 950, and 1000 nm) in front of the detection system, enable control of the exciting radiant power and remove second order diffractions. Dye solutions and NC dispersions in cuvettes are placed in the center of the sphere using a custom designed Spectraflect-coated cell holder.

(Fig. 3, right panel). For signal detection, we used an imaging spectrograph attached to a Peltier cooled, thinned back side illuminated deep depletion InGaAs CCD with high quantum efficiencies of >85% (1100–1500 nm). The N_2-purged spectrograph-detector ensemble was coupled to the integrating sphere with an IR-suitable quartz fiber bundle (LLB552-IR-0,12, IR Quartz, LOT Oriel, transmission >50%) shielded from direct reflexes with several baffles. We placed a filter wheel with neutral density (ND) filters (known wavelength-dependent transmission) in front of the integrating sphere for the control and variation of the incident radiant power and a filter wheel with several long pass (LP) interference filters (cut-on wavelengths of 600 nm, 800 nm, 950 nm, and 1000 nm) in front of the spectrograph–CCD ensemble to eliminate signal distorting second order diffractions and stray light. Dye solutions and NC dispersions in quartz cells were center-mounted in the sphere with a custom designed Spectraflect-coated cuvette holder positioned with a HeNe laser.

3.2 Setup characterization

We subsequently determined the wavelength accuracy of the excitation and detection channel(s), the linearity of the detection channel, and the wavelength-dependent spectral responsivity of the integrating sphere-spectrograph–CCD ensemble ($s(\lambda_{em})$).[46] The wavelength accuracy of the emission monochromator revealed maximum deviations <1.1 nm (see ESI, Fig. 3S†). Relative deviations from a linear behavior of the InGaAs CCD, measured at a constant integration time for varying excitation radiant powers, amounted to 0.3% (see ESI, Fig. 4S†) and for a constant radiant power and varying integration times to 0.5%. To reduce calibration uncertainties in $s(\lambda_{em})$ caused by stray light and second order effects and to account for the lack of suitable emission standards >950 nm, we employed two calibration lamps, a conventional spectral radiance transfer standard (SDS)[63] with an emission maximum at 1050 nm and a blackbody radiator (BBR) with a temperature-controlled spectral radiance, with an emission maximum at 1970 nm (for T = 1200 °C). An example of an emission correction curve (equaling $1/s(\lambda_{em})$) derived from the combination of these measurements (see ESI, Fig. 6S†) is shown in Fig. 2 (top panel; SDS: emission correction curve for 600–950 nm; BBR: emission correction curve measured for 950–1600 nm). The relative uncertainty for the determination of $s(\lambda_{em})$ from such combined calibration curves amounts to maximum 12%. This value includes uncertainties of the certified values of the calibrated light sources, the wavelength accuracy, linearity of the detection system, contributions from stray light, specific uncertainties arising from the different types of light sources and merging of the emission correction curves. Finally, the long term stability of the spectral radiant power of the different light sources of the integrating sphere setup was obtained as this is a critical parameter for all absolute measurements of Φ_f.[25] Multiple measurements over time using typical measurement conditions (integration time, number of accumulations; see ESI, Fig. 5S† for exemplary light sources) revealed relative deviations of the mean values (integration over the entire excitation peak) of <1%.

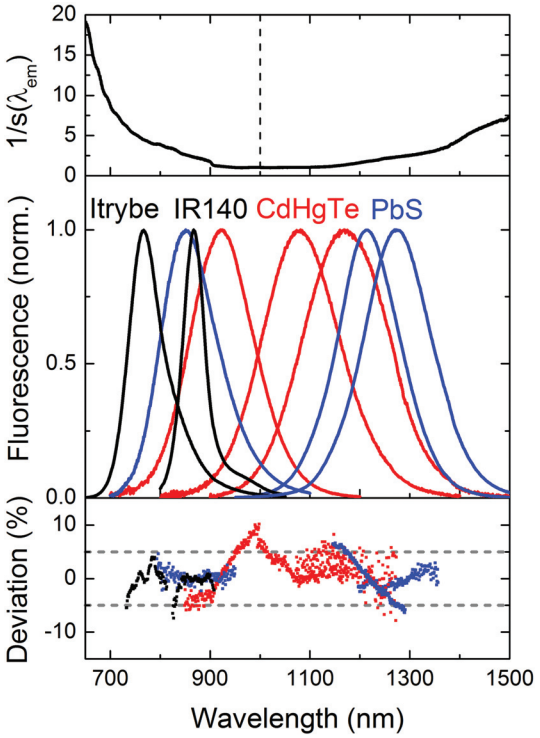

Fig. 2 Top: inverse spectral responsivity $1/s(\lambda_{em})$ of the NIR/IR integrating sphere setup determined with two calibration lamps. Middle: normalized corrected emission spectra of the NIR dyes Itrybe (solvent ethanol; black line) and IR140 (solvent DMSO; black line), MPA-stabilized CdHgTe NC colloids of various compositions and sizes dispersed in air-saturated D_2O (red lines), and PbS colloids of various sizes in TCE (blue lines) in air obtained with our NIR/IR integrating sphere setup. Bottom: relative spectral deviations between the corrected spectra measured with the integrating sphere setup and an independently calibrated spectrofluorometer (data given for intensities up to 50% of the intensity at the respective emission maximum). The dotted grey lines indicated relative deviations of 5%.

3.3 Setup validation – comparison of emission spectra

Proper validation of the calibration of the wavelength and intensity scale is the only way to obtain reliable emission spectra and Φ_f values. The good agreement between the emission correction curves obtained with SDS and BBR (see ESI, Fig. 6S†) provides already a first hint of the accuracy of our emission correction curve. For the control of $s(\lambda_{em})$ in the wavelength region of 600–1000 nm, we acquired the corrected emission spectra of the NIR dyes Itrybe and IR140 in ethanol and DMSO, respectively, and for 900–1600 nm, the corrected emission spectra of different IR-emissive semiconductor NCs, here mercaptopropionic acid (MPA)-stabilized $Cd_{1-x}Hg_xTe$ NCs of various compositions and sizes dispersed in D_2O and PbS colloids of various sizes in TCE with the NIR/IR sphere setup and our independently calibrated fluorometer. The generally good match between these emission spectra (Fig. 2, middle panel), indicated by the small relative spectral deviations of the order

of typically 5% (Fig. 2, lower panel), underlines the reliability of our emission correction curve.

3.4 Fluorescence quantum yields of NIR dyes with emission <1000 nm

Subsequently, we measured Φ_f of the NIR dyes Itrybe (solvent ethanol; emission: 680–950 nm; λ_{ex} = 633 nm)[64] and IR140 (solvent DMSO; emission: 830–1050 nm; λ_{ex} = 808 nm) with our NIR/IR and/or UV/vis/NIR integrating sphere setups and our calibrated fluorometer FSP920. Itrybe and IR140 were chosen because of their different Stokes shifts providing examples of small (Itrybe)[64] and large (IR140) spectral overlap between absorption and emission and their commercial availability in high purity as well as their subsequently derived good photochemical stability (see ESI, Fig. 9S†) and their excitation wavelength-independent Φ_f. The good agreement between the different methods and setups used underlines the reliability of Φ_f measurements with our new integrating sphere in the wavelength region of 630–1050 nm. We previously provided an uncertainty budget for Φ_f measurements in the wavelength region of 400–1000 nm.[9,24,25]

3.5 Reassessment of Φ_f of IR26 with emission >1000 nm

For the control of the reliability of Φ_f measurements >1000 nm, we chose IR26 in DCE (excitation range: 800–1000 nm, emission: 1010–1450 nm; see Fig. 3, left panel). Together with IR125 in DMSO, this dye presents the most common reference for red emissive NCs. Moreover, its Φ_f was only recently redetermined absolutely to be 4.8×10^{-4},[43] which is by a factor of *ca.* 10 lower than previously assumed,[44,45] rendering all Φ_f measured relative to this dye questionable.[39,40,42] Its extremely low Φ_f enables us to test the sensitivity of our new setup. Other challenges in the measurement of the Φ_f of IR26 are the strong spectral overlap between its absorption and emission bands favoring reabsorption and the absorption of the recommended solvent DCE within the dye's emission band with a sharp maximum at *ca.* 1170 nm (Fig. 3, left and right panels). Solvent absorption occurs for many common solvents >900 nm (Fig. 3, right); hence, uncertainties of determined quantum yields in this wavelength region exceed those of measurements at smaller wavelengths. Solvent and reabsorption effects are especially critical for integrating sphere measurements, as the size of the resulting signal distortions depends on the sphere diameter and reflectivity of the sphere coating as well as on the sample volume.

Table 1 Comparative absolute and relative measurements of Φ_f of the organic dyes Itrybe (λ_{ex} = 633 nm; relative to HITCI in ethanol, Φ_f = 0.30) and IR140 (λ_{ex} = 808 nm; relative to IR125 in DMSO, Φ_f = 0.23) emitting <1000 nm (Fig. 1) and IR26 (λ_{ex} = 980 nm; relative to IR125 in DMSO excited at 808 nm using a previously controlled excitation correction) emitting >1000 nm (Fig. 3, left panel); absolute 1: NIR/IR integrating sphere setup, absolute 2: UV/vis/NIR integrating sphere setup; relative: fluorometer FSP 920

Dye	Solvent	Φ_f Absolute 1	Φ_f Absolute 2	Φ_f Relative	Φ_f Lit.
Itrybe	EtOH	0.22	—	0.23	—
IR140	DMSO	0.20	0.20	0.20	—
IR26	DCE	0.0011	—	0.0007	0.00048

We determined the Φ_f of IR26 in DCE (see Table 1) absolutely at dye concentrations (c) of 0.7×10^{-6} to 6×10^{-6} mol L^{-1} (equaling absorbances of 0.09–0.80 at the absorption maximum of 1082 nm using a molar absorption coefficient $\varepsilon = 1.4 \times 10^{-5}$ L mol^{-1} cm^{-1} (ref. 65)) and with our spectrofluorometer relative to IR125 in DMSO[9,25] (IR26: λ_{ex} = 980 nm; IR125: λ_{ex} = 808 nm; see ESI, Fig. 2S†).[24,46] Absorption spectra of these dye solutions revealed the absence of dye aggregates at these concentrations (see ESI, Fig. 8S†) and the photochemical stability of IR26 was sufficient for excitation with a 980 nm laser diode (see ESI, Fig. 9S†). The sharp dip in the measured emission band of IR26 at *ca.* 1170 nm shown in Fig. 3 (left panel, red spectrum) demonstrates the considerable influence of solvent absorption. The influence of dye reabsorption on IR26 fluorescence follows from the red shift and the reduced intensity of the as-measured emission band compared to the reabsorption- and solvent-absorption-corrected fluorescence spectrum (Fig. 3, left panel, black spectrum). This is reflected by the corresponding Φ_f data, *i.e.*, a Φ_f of 0.7×10^{-3} as measured, which amounts to 1.1×10^{-3} after consideration of solvent absorption and dye reabsorption (see ESI;† Fig. 8S).[9,24,25] We determined the relative uncertainty of this

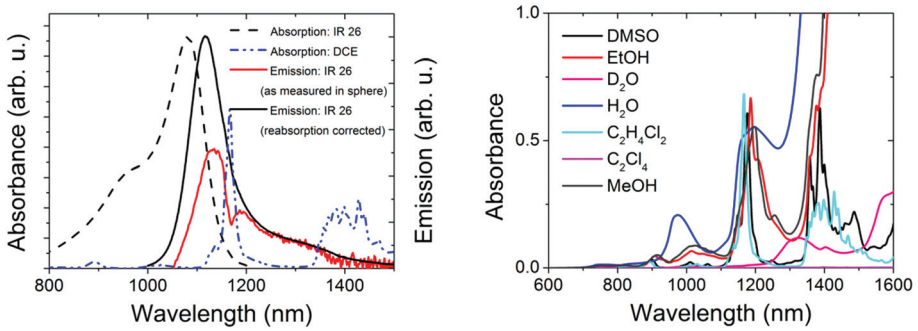

Fig. 3 Left: normalized absorption and emission spectra of IR26 in DCE (without and with corrections for dye reabsorption and solvent absorption) and absorption of the solvent DCE within the wavelength region of dye emission. Right: absorption spectra of common organic solvents, H_2O, and D_2O used for the study of IR dyes and NCs, given for an optical path length of 1 cm.

value to be 21% (2.3×10^{-4}). This includes contributions from setup calibration (12%) and applied corrections (15%) as well as the relative standard deviation of fluorescence measurements with our NIR/IR integrating sphere setup (9%). Relative measurements yielded a Φ_f of 0.7×10^{-3} (Table 1). We estimated the relative uncertainty of this value to be 30% (2.1×10^{-4}) taking into account uncertainties from instrument calibration (emission correction from the instrument manufacturer, two point self-made excitation correction, and Φ_f uncertainty of the reference dye IR125), dye reabsorption and solvent absorption and the relative standard deviation of fluorescence measurements. Dye purity was not considered in both cases.

We attribute our finding of a higher Φ_f for IR26 than the value of 0.48×10^{-3} reported by Semonin *et al.*[43] to different calibration and correction procedures. Nevertheless, our value still equals the absolute upper limit of Φ_f of this dye assumed by Semonin. In addition, the fact that we could measure Φ_f absolutely at concentrations of 0.7×10^{-6} to 6×10^{-6} mol L^{-1} demonstrates the higher sensitivity of our integrating sphere setup compared to the setup reported by Semonin *et al.* who used dye concentrations of 2×10^{-6} to 11×10^{-6} mol L^{-1} (equaling the absorbances of 0.3–1.5 at the absorption maximum of 1082 nm) for the integration sphere measurement of Φ_f of IR26. In this respect, the measurement uncertainties given by us for the absolute determination of Φ_f of IR26 exceed only apparently the uncertainty provided by Semonin *et al.* of 0.2×10^{-4} (equaling a relative uncertainty of 4.2%) that was not really deduced from the actual integrating sphere measurements. This uncertainty was derived by Semonin *et al.* only from a fit considering dye reabsorption, but not solvent absorption, which was made for a 0°/90° measurement geometry and not for the integrating sphere measurements. Most likely, the small uncertainties given by Semonin *et al.* consider solely the standard deviation of the fluorescence measurements, but not a complete uncertainty budget as given by us.[24,25]

Nevertheless, our data verify the considerable overestimation of many Φ_f of NIR- and IR-emissive NCs like PbS, PbSe, and $Cd_{1-x}Hg_xTe$.[39,40,42] This finding, together with the Φ_f values absolutely measured for PbS in different solvents of the order of 0.05 to 0.60[43,66–68] and relative to IR125 (using a reference Φ_f of 0.13)[38] of the order of 0.20 to 0.40,[33,35] clearly demonstrates the need for a critical reexamination of Φ_f values of representative IR-emissive semiconductor NCs.

3.6 Φ_f of IR-emissive semiconductor $Cd_{1-x}Hg_xTe$ ternary alloys

Especially promising IR-emissive NCs are $Cd_{1-x}Hg_xTe$ ternary alloys as well as PbS and PbSe.[3,33,42,55–57] As PbSe NCs can be more prone to surface oxidation as PbS NCs,[69–72] we decided to evaluate only the Φ_f of dispersions of representative $Cd_{1-x}Hg_xTe$ ternary alloys of different compositions and sizes and exemplary differently sized PbS colloids detailed in the following section to provide examples of achievable Φ_f values for IR-emissive quantum dots and to identify NC-specific challenges and sources of uncertainty.

We determined the Φ_f of three MPA-capped $Cd_xHg_{1-x}Te$ NC samples with comparatively broad emission spectra in D_2O spanning a wavelength region of *ca.* 750–1350 nm shown in Fig. 2 and 4 (inset) at different excitation wavelengths between 633 and 785 nm relatively and absolutely. Prior to these measurements, we measured time traces with our integrating sphere setup to exclude photodecomposition and photobrightening for excitation with intense laser diodes, the radiant flux of which considerably exceeded that of a xenon lamp monochromator ensemble used for relative photoluminescence measurements. Moreover, Φ_f were determined relatively before and after each absolute measurement. These studies did not reveal light-induced changes of the $Cd_{1-x}Hg_xTe$ NC colloids.

As follows from Fig. 4, the absolutely and relatively determined Φ_f of the three $Cd_{1-x}Hg_xTe$ colloids agree reasonably well. We determined the relative uncertainties of absolutely measured Φ_f to be 16%, considering uncertainty contributions of setup calibration (12%) and applied reabsorption and stray

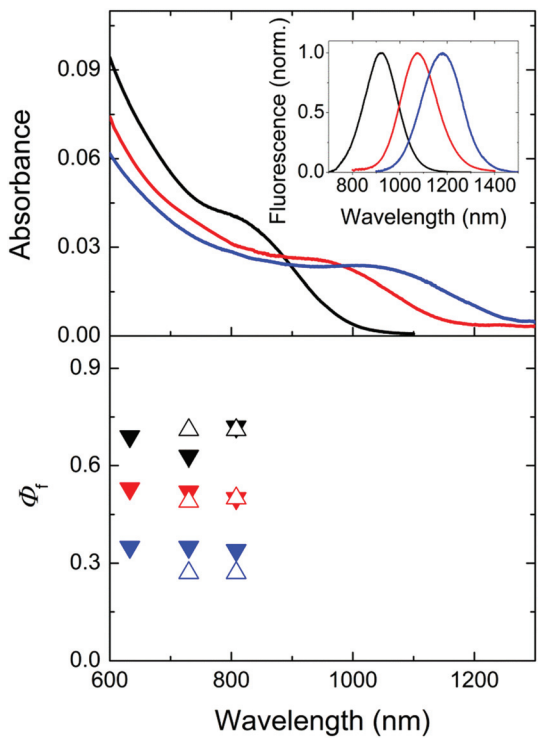

Fig. 4 Top: normalized absorption spectra of three representative $Cd_{1-x}Hg_xTe$ NC colloids of different sizes and compositions (black: 4.8. nm, Cd : Hg = 99 : 1, $c = 1.3 \times 10^{-6}$ mol L^{-1}; red: 6.3 nm, Cd : Hg = 98 : 2, $c = 1.3 \times 10^{-6}$ mol L^{-1}; blue: 7.1 nm, Cd : Hg = 97 : 3, $c = 5.2 \times 10^{-7}$ mol L^{-1}) in D_2O in air. The corresponding corrected emission spectra are shown in the inset and in Fig. 2 (middle panel). The concentration of the $Cd_{1-x}Hg_xTe$ NC was determined by measuring the concentration of the respective metal ions (Cd^{2+} and Hg^{2+}) *via* ICP-OES as previously described[15,73] and considering the NC diameter derived from TEM data. Bottom: absolutely measured Φ_f (solid symbols) and relatively measured Φ_f (open symbols) at different excitation wavelengths. Considering the uncertainties of both methods, the determined values overlap.

light corrections (5%; see ESI†) as well as of the relative standard deviation of fluorescence measurements with the NIR/IR integrating sphere setup (10%). The uncertainties of relatively measured Φ_f are estimated to be 15% (no excitation correction, only small absorption of D_2O, less pronounced reabsorption as found for IR26). None of the colloids studied showed a dependence of its Φ_f on the excitation wavelength within the uncertainties. The comparatively high Φ_f between *ca.* 0.3 and 0.65 of our colloids underline the suitability of our simple one pot aqueous synthesis[42] for the preparation of bright $Cd_xHg_{1-x}Te$ NCs especially with the ligand MPA.[73] Whether the observed trend of a decrease in Φ_f with increasing size and/or Hg content is really representative, possibly originating from a confinement reduction with increasing particle size and/or the introduction of an increasing number of crystal and surface defects with larger numbers of Hg^{2+} ions (with sizes exceeding that of Cd^{2+}) favoring luminescence quenching, remains to be shown for a larger set of samples.

3.7 Aging studies and Φ_f of IR-emissive PbS colloids

Subsequently, we investigated the spectroscopic properties of three oleate-capped PbS colloids of different sizes, *i.e.*, 2.3 nm, 4.1 nm, and 4.4 nm, in TCE which does not absorb within the wavelength region of NC emission (Fig. 2 and 3, right panel; ESI, Fig. 10S†). To account for a possible influence of oxygen and hence NC oxidation, which is manifested by a blue shift in absorption and emission and can depend on particle size,[72] the 4.4 nm-sized PbS colloid batch was split into two portions immediately after synthesis. One portion was kept always under inert gas and the other sample was stored in air.

PbS aging. Spectroscopic studies of our differently sized PbS colloids kept in air and dispersed in TCE revealed a blue shift of the absorption and emission maxima with time in conjunction with a considerable narrowing of the blue shifted absorption band and a reduction in emission bandwidth, *i.e.*, FWHM (full width at half height of the maximum). This is exemplarily shown for 4.4 nm PbS NCs in Fig. 5 (top panel and lower panels), the largest NC of this series, which underwent the most pronounced changes (see ESI, Fig. 11S†). Here, the initial emission maximum located at 1380 nm shifted to 1265 nm over a period of *ca.* 250 days, accompanied by a considerable narrowing of the absorption band (Fig. 5, lower panel, left; comparison of black and blue solid spectra) and the emission band (Fig. 5, lower panel, right; initial FWHM of 250 nm (0.165 eV) developing into FWHM of 150 nm (0.113 eV)). Simultaneously, Φ_f increased from 0.24 to 0.45 within 250 days and then remained stable (Fig. 5, top). These Φ_f values lay at the upper end of the Φ_f values reported by Semonin *et al.*,[43] underlining the good quality of our PbS NCs. This is similarly true for the two smaller PbS NC samples that showed a higher stability to aging, as indicated by their smaller time-dependent spectral shifts in absorption and emission and changes in FWHM (see ESI, Fig. 11S†). The smallest 2.3 nm-sized PbS particles reached a stable state almost immediately after synthesis (FWHM = 0.178 eV, no time-dependent changes). We attribute this size-dependent stability of our three PbS colloids to similar effects to those reported by Choi *et al.* for oleate-capped PbS nanoparticles.[72] They claimed a size-dependent shape transition from air stable ligand-passivated (111) facets-only octahedra to (111)/(100) cubooctahedra with bare self-passivated (100) facets which are prone to surface oxidation.[72] The latter is reflected by the strong aging-induced changes in the optical properties of especially the 4.4 nm PbS NCs (Fig. 5) which can be attributed to surface etching. Etching leads to a decrease of the PbS core size and the formation of an oxidized layer ($PbSO_x$) on the surface of the PbS NC as recently reported by, *e.g.*, Tang *et al.*[74] and Hardman *et al.*[75] in conjunction with a focusing of the NC size distribution, indicated by the narrowing of the absorption and emission bands, that is possibly accompanied by a shape transition. Such a shape transition was observed, *e.g.*, by Hines *et al.*[33] The astonishing luminescence enhancement in air for our PbS NCs and size regime, contradicting other studies of photobrightening and photodarkening of PbS NCs where irreversible oxidation-induced luminescence quenching was observed,[76] suggests a passivation of surface defects by this surface oxidation. In addition, the efficiency of the "intrinsic" nonradiative interband recombination caused by the increase in bandgap in oxidized, *i.e.*, smaller PbS NCs, could also be reduced.[43]

Our explanation for the aging-induced luminescence enhancement is supported by the improved stability of 4.4 nm PbS NCs kept under inert gas. This is reflected by only very small time-dependent changes in the spectral position of the emission maximum located at 1390 nm, matching the initial value found for the freshly synthesized 4.4 nm PbS NC in the presence of oxygen (Fig. 5, upper panel), and its considerably smaller Φ_f of 0.15.

Photostability and Φ_f of PbS. Within the context of the desired validation of absolute measurements of photoluminescence with our new integrating sphere setup, we measured the Φ_f of aged PbS NC colloids (4.4 nm PbS NCs stored both in air and under inert gas) at different excitation wavelengths relatively and absolutely with different excitation radiant powers. Relative measurements with excitation radiant powers of 0.1 mW in the wavelength region of 690 nm to 915 nm (see ESI, Fig. 2S†) revealed no or only very small light-induced changes in absorption and emission as well as excitation wavelength-independent Φ_f. Absolute fluorescence measurements with the exemplarily chosen more intense 808 nm laser, however, revealed radiant power-dependent photoeffects for all three PbS NCs, which affect the resulting Φ_f values. This is exemplarily shown for 4.4 nm PbS NCs aged in air for *ca.* 300 days (Fig. 5, middle panel, right) and stored under an inert gas atmosphere (Fig. 5, middle panel, left). For 4.4 nm PbS in air, Φ_f decreased at short illumination times and subsequently increased again, reaching almost the starting Φ_f value. Simultaneously, its absorption and emission are blue shifted by *ca.* 10 nm (Fig. 5, lower panels, blue spectra), indicative of slight photocorrosion. Similar photoeffects, *i.e.*, photobrightening and photodarkening, commonly ascribed to (reversible) trapping of carriers to a long-lived, optically dark state or particle charging, have been already reported for PbS

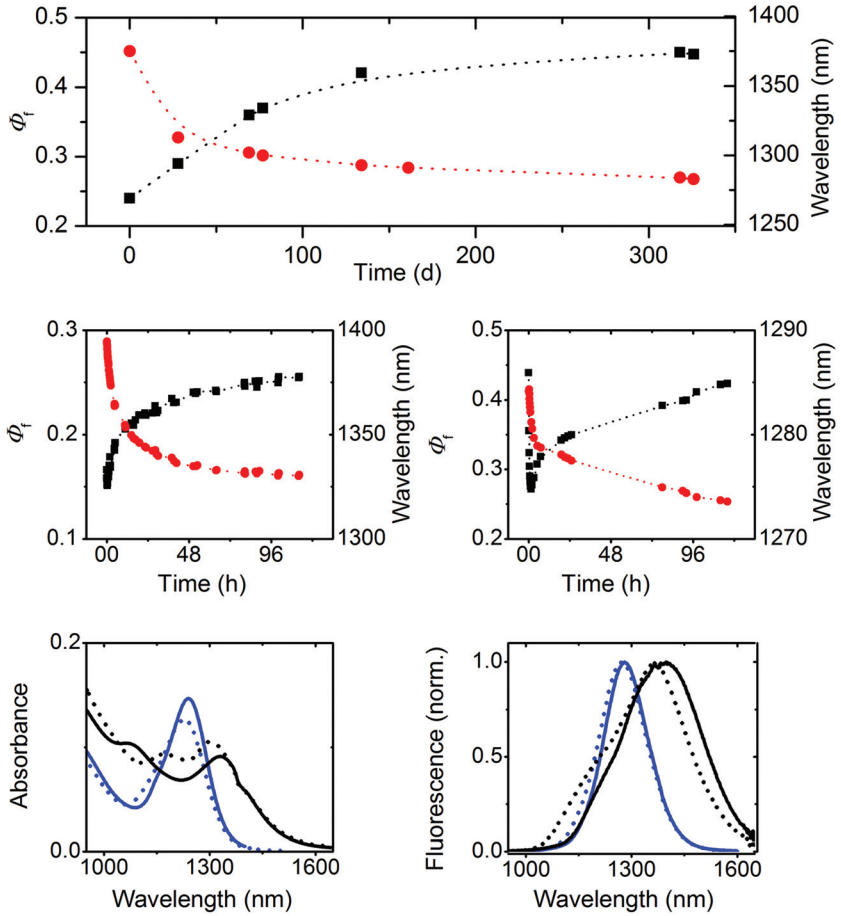

Fig. 5 Top: aging of 4.4 nm PbS NCs in air. Blue shift of the spectral position of the emission band (red circles) and the relatively measured Φ_f (black squares) of 4.4 nm PbS NCs as a function of time after colloid preparation. Middle: absolutely measured Φ_f and photoeffects. Change in absolutely measured Φ_f (black squares) and in the spectral position of the emission band (red circles) of 4.4 nm PbS NCs kept under inert gas (left panel) and of 4.4 nm PbS NCs, both aged in air for *ca.* 300 days, as a function of illumination time. Illumination was performed with the 808 nm laser diode of the integrating sphere setup (radiant power of 62 mW). Bottom: aging and light-induced spectral changes. Change in the absorption spectra (left panel) of 4.4 nm PbS NCs aged/stored under inert gas for *ca.* 300 days (black) and in air (blue) and diluted with TCE, before (solid lines) and after illumination (dashed lines) with the 808 nm laser diode (radiant power of 62 mW) for 120 hours. The initial absorption spectrum of 4.4 nm PbS NCs stored under an inert gas atmosphere (black solid line) closely matches the initial absorption spectrum of this colloid prior to aging in air (top panel).

quantum dots.[76] Illumination of 4.4 nm PbS NCs in the absence of oxygen leads to a blue shift in absorption and especially in emission by about 50 nm (Fig. 5, lower panels, black spectra) and an increase in Φ_f by a factor of almost two (Fig. 5, middle panel, left). The eventually reached Φ_f of 0.27 is, however, still clearly smaller than the Φ_f of 0.45 obtained for the same PbS colloid in air (Fig. 5, upper panel). Purging of the solution of the air-aged PbS NCs with argon did not alter the light-induced spectroscopic changes revealed by this colloid, still showing photodarkening followed by photobrightening upon light exposure. Apparently, aging in air changed the NC surface chemistry irreversibly, which confirms the formation of a $PbSO_x$ layer at the NC surface as reported, *e.g.*, by Tang *et al.*[74] and Hardman *et al.*[75]

Similar experiments with 2.3 nm and 4.1 nm PbS NCs in air (see ESI, Fig. 12S†) revealed size-dependent photoeffects. The smallest PbS colloid showed solely photobrightening, leading to an increase of the initially obtained Φ_f of 0.18 to 0.71, accompanied by a blue shift of the emission band from 958 nm to 920 nm. At lower radiant powers, also fast photodarkening was observed, yet in all cases, subsequent photobrightening dominated, always yielding similarly high Φ_f. In contrast, 4.1 nm PbS NCs showed a similar behavior to 4.4 nm PbS particles and comparable Φ_f. These size-dependent differences in photochemical behavior seem to correlate with the size-dependent aging of these colloids, providing a further hint of a different surface chemistry of our three PbS NCs.

Comparison of absolute and relative Φ_f measurements for PbS. As exemplarily shown for our 4.4 nm PbS colloid in air and under an inert gas atmosphere, principally the absolutely measured initial Φ_f values agree reasonably well with the relatively obtained data (see, *e.g.*, Fig. 5; finally reached Φ_f after 300 days in the top panel and the starting Φ_f value in the middle right panel for PbS in air and for PbS under inert gas,

the initial Φ_f after synthesis from the top panel and the starting Φ_f value in the middle left panel, respectively). The desired comparison of relatively and absolutely measured Φ_f data for PbS is, however, hampered by the radiant power- and size-dependent photodarkening and photobrightening of this material, since these measurements are commonly performed at different excitation radiant powers (see ESI†). Our results are nevertheless very interesting for a better understanding of the factors yielding very bright PbS NCs. In this respect, it should be kept in mind that the measurement conditions used by us for the absolute determination of Φ_f of the PbS NCs most likely closely mimic those of absolute measurements reported by other groups in the IR wavelength region. Integrating sphere measurements with IR-emissive NCs like lead chalcogenides are commonly performed with intense excitation light sources like a 831 nm semiconductor laser,[67,68,77] LEDs emitting at 850 nm or 950 nm,[43] or a 405 nm laser,[78] with no information provided on the excitation radiant powers employed. There are only very few reports of integrating sphere setups for measurements >1000 nm using a fiber coupled xenon lamp–monochromator ensemble as a less intense excitation light source.[79] Hence, measurement condition- and material-specific photo-induced changes in fluorescence intensity as found by us for PbS NCs could principally also affect other literature data, especially in the case of potentially oxygen- and light-sensitive lead chalcogenides.

4 Conclusions and outlook

In summary, we presented the design of a new integrating sphere setup for spectrally resolved measurements of absolute photoluminescence quantum yields (Φ_f) of barely to moderately emissive organic dyes to highly emissive semiconductor NCs in the wavelength region of 600–1600 nm and addressed common instrument- and material-related challenges for fluorescence measurements in the NIR and IR and solutions. We demonstrated the reliability of our measurements by comparing the corrected emission spectra and the relatively and absolutely determined Φ_f of several organic dyes, MPA-capped $Cd_{1-x}Hg_xTe$ in D_2O, and oleate-capped PbS NCs in TCE obtained with two integrating sphere setups and a spectrofluorometer, all independently calibrated. These validation strategies provide a good example of the validation of challenging fluorescence measurements in the NIR and IR for, *e.g.*, semiconductor quantum dots and rods, carbon nanotubes, and upconversion materials.

Moreover, we redetermined the Φ_f of the only IR reference dye IR26 to be 1.1×10^{-3} with an uncertainty of 2.3×10^{-4} derived from an uncertainty budget and introduced a procedure for the simultaneous correction for sample reabsorption and solvent absorption. These effects present common signal distortions in the IR. A further reduction in measurement uncertainties requires especially an improved stability of the excitation light sources used for our NIR/IR integrating sphere setup. We could verify the high Φ_f of 0.3 to 0.7 for high quality aqueous $Cd_{1-x}Hg_xTe$ NC colloids prepared *via* our previously reported simple one pot synthesis. For differently sized oleate-capped PbS colloids with Φ_f between 0.2 and 0.7, we demonstrated the influence of quantum dot-inherent photobrightening and photodarkening on Φ_f measurements, which can be material-specific, size-dependent, and affected by oxygen. These effects, which can be expected also, *e.g.* for other lead chalcogenides, together with the considerable overassessment of many previously published Φ_f of NIR- and IR-emissive quantum dots like PbS, PbSe, and $Cd_{1-x}Hg_xTe$ derived from our reexamined Φ_f of the reference dye IR26 underline the need for a critical reevaluation of Φ_f values of IR-emissive nanomaterials. A critical evaluation of Φ_f data and procedures used for the determination of Φ_f is generally of considerable importance with respect to the foreseeable increasing importance of luminescence measurements in the wavelength region of 1000–1600 nm, *e.g.* for bioimaging studies. This similarly triggers the need for broadly available and well characterized quantum yield standards also for this wavelength region.

Acknowledgements

We express our gratitude to Dr Markus Grabolle (BAM) for many fruitful discussions, to Dipl.-Ing A. Güttler (BAM) for technical assistance during the calibration of the spectrofluorometer FSP920, to Frau M. Spieles (BAM) for the HPLC measurements of the dyes, and Christine Damm (IFW Dresden e.V.) for the supports by the TEM measurements. We gratefully acknowledge financial support from the Deutsche Forschungsgemeinschaft (DFG; grants RE-1203/12-1 and EY 16/14-1).

References

1 B. Valeur, *Molecular Fluorescence: Principles and Application*, Wiley-VCH, Weinheim, 2002.
2 D. M. Jameson, J. C. Croney and P. D. J. Moens, *Biophotonics, Pt A*, 2003, **360**, 1–43.
3 S. V. Kershaw, A. S. Susha and A. L. Rogach, *Chem. Soc. Rev.*, 2013, **42**, 3033–3087.
4 M. T. Harrison, S. V. Kershaw, M. G. Burt, A. L. Rogach, A. Kornowski, A. Eychmüller and H. Weller, *Pure Appl. Chem.*, 2000, **72**, 295–307.
5 P. V. Kamat, *J. Phys. Chem. C*, 2008, **112**, 18737–18753.
6 E. H. Sargent, *Adv. Mater.*, 2005, **17**, 515–522.
7 M. Graetzel, R. A. J. Janssen, D. B. Mitzi and E. H. Sargent, *Nature*, 2012, **488**, 304–312.
8 U. Resch-Genger, M. Grabolle, S. Cavaliere-Jaricot, R. Nitschke and T. Nann, *Nat. Methods*, 2008, **5**, 763–775.
9 C. Würth, M. Grabolle, J. Pauli, M. Spieles and U. Resch-Genger, *Nat. Protocols*, 2013, **8**, 1535–1550.
10 S. E. Braslavsky, *Pure Appl. Chem.*, 2007, **79**, 293–465.
11 U. Resch-Genger and K. Rurack, *Pure Appl. Chem.*, 2013, **85**, 2005–2026.

12 C. T. Xu, Q. Q. Zhan, H. C. Liu, G. Somesfalean, J. Qian, S. L. He and S. Andersson-Engels, *Laser Photonics Rev.*, 2013, **7**, 663–697.
13 S. L. Gai, C. X. Li, P. P. Yang and J. Lin, *Chem. Rev.*, 2014, **114**, 2343–2389.
14 M. Grabolle, M. Spieles, V. Lesnyak, N. Gaponik, A. Eychmüller and U. Resch-Genger, *Anal. Chem.*, 2009, **81**, 6285–6294.
15 S. Leubner, S. Hatami, N. Esendemir, T. Lorenz, J. O. Joswig, V. Lesnyak, S. Recknagel, N. Gaponik, U. Resch-Genger and A. Eychmüller, *Dalton Trans.*, 2013, **42**, 12733–12740.
16 J. C. Boyer, M. P. Manseau, J. I. Murray and F. van Veggel, *Langmuir*, 2010, **26**, 1157–1164.
17 F. Wang, J. A. Wang and X. G. Liu, *Angew. Chem., Int. Ed.*, 2010, **49**, 7456–7460.
18 J. Ziegler, A. Merkulov, M. Grabolle, U. Resch-Genger and T. Nann, *Langmuir*, 2007, **23**, 7751–7759.
19 L. H. Qu and X. G. Peng, *J. Am. Chem. Soc.*, 2002, **124**, 2049–2055.
20 J. B. Delehanty, K. Susumu, R. L. Manthe, W. R. Algar and I. L. Medintz, *Anal. Chim. Acta*, 2012, **750**, 63–81.
21 X. H. Ji, D. Copenhaver, C. Sichmeller and X. G. Peng, *J. Am. Chem. Soc.*, 2008, **130**, 5726–5735.
22 G. Kalyuzhny and R. W. Murray, *J. Phys. Chem. B*, 2005, **109**, 7012–7021.
23 C. Wang, X. Gao and X. Su, *Anal. Bioanal. Chem.*, 2010, **397**, 1397–1415.
24 C. Würth, M. Grabolle, J. Pauli, M. Spieles and U. Resch-Genger, *Anal. Chem.*, 2011, **83**, 3431–3439.
25 C. Würth, J. Pauli, C. Lochmann, M. Spieles and U. Resch-Genger, *Anal. Chem.*, 2012, **84**, 1345–1352.
26 C. Würth, M. G. Gonzalez, R. Niessner, U. Panne, C. Haisch and U. R. Genger, *Talanta*, 2012, **90**, 30–37.
27 K. Suzuki, A. Kobayashi, S. Kaneko, K. Takehira, T. Yoshihara, H. Ishida, Y. Shiina, S. Oishi and S. Tobita, *Phys. Chem. Chem. Phys.*, 2009, **11**, 9850–9860.
28 K. Rurack, in *Standardization and Quality Assurance in Fluorescence Measurements I: Techniques*, ed. U. Resch-Genger, Springer, Berlin-Heidelberg, 2008, vol. 5.
29 D. F. Eaton, *Pure Appl. Chem.*, 1988, **60**, 1107–1114.
30 A. M. Brouwer, *Pure Appl. Chem.*, 2011, **83**, 2213–2228.
31 J. R. Lakowicz, *Principles of fluorescence spectroscopy*, Springer Science+Business Media, LLC, New York, 3rd edn, 2006.
32 J. N. Demas and G. A. Crosby, *J. Phys. Chem.*, 1971, **75**, 991–1024.
33 M. A. Hines and G. D. Scholes, *Adv. Mater.*, 2003, **15**, 1844–1849.
34 H. Du, C. L. Chen, R. Krishnan, T. D. Krauss, J. M. Harbold, F. W. Wise, M. G. Thomas and J. Silcox, *Nano Lett.*, 2002, **2**, 1321–1324.
35 L. Cademartiri, J. Bertolotti, R. Sapienza, D. S. Wiersma, G. von Freymann and G. A. Ozin, *J. Phys. Chem. B*, 2006, **110**, 671–673.
36 J. J. Peterson and T. D. Krauss, *Nano Lett.*, 2006, **6**, 510–514.
37 F. Q. Ren, H. G. Zhao, F. Vetrone and D. L. Ma, *Nanoscale*, 2013, **5**, 7800–7804.
38 R. C. Benson and H. A. Kues, *Phys. Med. Biol*, 1978, **23**, 159–163.
39 J. E. Murphy, M. C. Beard, A. G. Norman, S. P. Ahrenkiel, J. C. Johnson, P. R. Yu, O. I. Micic, R. J. Ellingson and A. J. Nozik, *J. Am. Chem. Soc.*, 2006, **128**, 3241–3247.
40 B. L. Wehrenberg, C. J. Wang and P. Guyot-Sionnest, *J. Phys. Chem. B*, 2002, **106**, 10634–10640.
41 M. V. Kovalenko, R. D. Schaller, D. Jarzab, M. A. Loi and D. V. Talapin, *J. Am. Chem. Soc.*, 2012, **134**, 2457–2460.
42 V. Lesnyak, A. Lutich, N. Gaponik, M. Grabolle, A. Plotnikov, U. Resch-Genger and A. Eychmüller, *J. Mater. Chem.*, 2009, **19**, 9147–9152.
43 O. E. Semonin, J. C. Johnson, J. M. Luther, A. G. Midgett, A. J. Nozik and M. C. Beard, *J. Phys. Chem. Lett.*, 2010, **1**, 2445–2450.
44 W. Kranitzky, B. Kopainsky, W. Kaiser, K. H. Drexhage and G. A. Reynolds, *Opt. Commun.*, 1981, **36**, 149–152.
45 B. Kopainsky, P. Qiu, W. Kaiser, B. Sens and K. H. Drexhage, *Appl. Phys. B*, 1982, **29**, 15–18.
46 U. Resch-Genger and P. C. DeRose, *Pure Appl. Chem.*, 2012, **84**, 1815–1835.
47 C. Würth, C. Lochmann, M. Spieles, J. Pauli, K. Hoffmann, T. Schuttrigkeit, T. Franzl and U. Resch-Genger, *Appl. Spectrosc.*, 2010, **64**, 733–741.
48 S. H. Xu, C. L. Wang, Q. Y. Xu, R. Q. Li, H. B. Shao, H. S. Zhang, M. Fang, W. Lei and Y. P. Cui, *J. Phys. Chem. C*, 2010, **114**, 14319–14326.
49 T. V. Duncan, M. A. M. Polanco, Y. Kim and S. J. Park, *J. Phys. Chem. C*, 2009, **113**, 7561–7566.
50 D. Tonti, F. van Mourik and M. Chergui, *Nano Lett.*, 2004, **4**, 2483–2487.
51 R. A. Cruz, V. Pilla and T. Catunda, *J. Appl. Phys.*, 2010, 107.
52 Z. M. Tao, G. S. Hong, C. Shinji, C. X. Chen, S. Diao, A. L. Antaris, B. Zhang, Y. P. Zou and H. J. Dai, *Angew. Chem., Int. Ed.*, 2013, **52**, 13002–13006.
53 G. Hong, S. Diao, J. Chang, A. L. Antaris, C. Chen, B. Zhang, S. Zhao, D. N. Atochin, P. L. Huang, K. I. Andreasson, C. J. Kuo and H. Dai, *Nat. Photonics*, 2014, **8**, 723–730.
54 D. Salo, H. R. Zhang, D. M. Kim and M. Y. Berezin, *J. Biomed. Opt.*, 2014, 19.
55 V. Lesnyak, N. Gaponik and A. Eychmüller, *Chem. Soc. Rev.*, 2013, **42**, 2905–2929.
56 S. Gupta, O. Zhovtiuk, A. Vaneski, Y.-C. Lin, W.-C. Chou, S. V. Kershaw and A. L. Rogach, *Part. Part. Syst. Charact.*, 2013, **30**, 346–354.
57 E. H. Sargent, *Nat. Photonics*, 2012, **6**, 133–135.
58 J. Poppe, S. Gabriel, L. Liebscher, S. G. Hickey and A. Eychmüller, *J. Mater. Chem. C*, 2013, **1**, 1515–1524.
59 L. Cademartiri, E. Montanari, G. Calestani, A. Migliori, A. Guagliardi and G. A. Ozin, *J. Am. Chem. Soc.*, 2006, **128**, 10337–10346.
60 P. C. DeRose and U. Resch-Genger, *Anal. Chem.*, 2010, **82**, 2129–2133.

61 U. Resch-Genger, D. Pfeifer, C. Monte, W. Pilz, A. Hoffmann, M. Spieles, K. Rurack, J. Hollandt, D. Taubert, B. Schonenberger and P. Nording, *J. Fluoresc.*, 2005, **15**, 315–336.
62 J. C. de Mello, H. F. Wittmann and R. H. Friend, *Adv. Mater.*, 1997, **9**, 230–232.
63 U. Resch-Genger, W. Bremser, D. Pfeifer, M. Spieles, A. Hoffmann, P. C. DeRose, J. C. Zwinkels, F. o. Gauthier, B. Ebert, R. D. Taubert, C. Monte, J. Voigt, J. Hollandt and R. Macdonald, *Anal. Chem.*, 2012, **84**, 3889–3898.
64 T. Behnke, J. E. Mathejczyk, R. Brehm, C. Würth, F. R. Gomes, C. Dullin, J. Napp, F. Alves and U. Resch-Genger, *Biomaterials*, 2013, **34**, 160–170.
65 D. Brown and D. Benfey, *Comprehensive Study of Diode-Pumped Dye Lasers. Phase 1*, 1991.
66 S. Hinds, S. Myrskog, L. Levina, G. Koleilat, J. Yang, S. O. Kelley and E. H. Sargent, *J. Am. Chem. Soc.*, 2007, **129**, 7218–7219.
67 L. Bakueva, I. Gorelikov, S. Musikhin, X. S. Zhao, E. H. Sargent and E. Kumacheva, *Adv. Mater.*, 2004, **16**, 926–929.
68 X. S. Zhao, I. Gorelikov, S. Musikhin, S. Cauchi, V. Sukhovatkin, E. H. Sargent and E. Kumacheva, *Langmuir*, 2005, **21**, 1086–1090.
69 M. Sykora, A. Y. Koposov, J. A. McGuire, R. K. Schulze, O. Tretiak, J. M. Pietryga and V. I. Klimov, *ACS Nano*, 2010, **4**, 2021–2034.
70 J. W. Stouwdam, J. Shan, F. van Veggel, A. G. Pattantyus-Abraham, J. F. Young and M. Raudsepp, *J. Phys. Chem. C*, 2007, **111**, 1086–1092.
71 I. Moreels, Y. Justo, B. De Geyter, K. Haustraete, J. C. Martins and Z. Hens, *ACS Nano*, 2011, **5**, 2004–2012.
72 H. Choi, J.-H. Ko, Y.-H. Kim and S. Jeong, *J. Am. Chem. Soc.*, 2013, **135**, 5278–5281.
73 S. Leubner, R. Schneider, A. Dubavik, S. Hatami, N. Gaponik, U. Resch-Genger and A. Eychmüller, *J. Mater. Chem. C*, 2014, **2**, 5011–5018.
74 J. Tang, L. Brzozowski, D. A. R. Barkhouse, X. Wang, R. Debnath, R. Wolowiec, E. Palmiano, L. Levina, A. G. Pattantyus-Abraham, D. Jamakosmanovic and E. H. Sargent, *ACS Nano*, 2010, **4**, 869–878.
75 S. J. O. Hardman, D. M. Graham, S. K. Stubbs, B. F. Spencer, E. A. Seddon, H.-T. Fung, S. Gardonio, F. Sirotti, M. G. Silly, J. Akhtar, P. O'Brien, D. J. Binks and W. R. Flavell, *Phys. Chem. Chem. Phys.*, 2011, **13**, 20275–20283.
76 J. J. Peterson and T. D. Krauss, *Phys. Chem. Chem. Phys.*, 2006, **8**, 3851–3856.
77 T. W. F. Chang, A. Maria, P. W. Cyr, V. Sukhovatkin, L. Levina and E. H. Sargent, *Synth. Met.*, 2005, **148**, 257–261.
78 J. S. Steckel, S. Coe-Sullivan, V. Bulovic and M. G. Bawendi, *Adv. Mater.*, 2003, **15**, 1862–1866.
79 E. Lifshitz, M. Brumer, A. Kigel, A. Sashchiuk, M. Bashouti, M. Sirota, E. Galun, Z. Burshtein, A. Q. Le Quang, I. Ledoux-Rak and J. Zyss, *J. Phys. Chem. B*, 2006, **110**, 25356–25365.